

SIGNATURES OF PARTICLE DECAY IN 21 CM ABSORPTIONS FROM FIRST MINIHALOS

EVGENII O. VASILIEV AND YURI A. SHCHEKINOV

Southern Federal University, Stachki Ave. 194, Rostov-on-Don, 344090 Russia

Draft version September 15, 2018

ABSTRACT

The imprint of decaying dark matter (DM) particles in characteristics of the “21 cm forest” – absorptions in 21 cm from minihalos in spectra of distant radio-loud sources – is considered within a 1D self-consistent hydrodynamic description of minihalos from their turnaround point to virialization. The most pronounced influence of decaying DM on evolution of minihalos is found in the mass range $M = 10^5 - 10^6 M_\odot$, for which unstable DM with the current upper limit of the ionization rate $\xi_L = 0.59 \times 10^{-25} \text{ s}^{-1}$ depresses 21 cm optical depth by an order of magnitude compared to the standard recombination scenario. Even rather a modest ionization $\xi \sim 0.3\xi_L$ practically “erases” absorption features and results in a considerable decrease (by factor of more than 2.5) of the number of strong ($W_\nu^{obs} \gtrsim 0.3 \text{ kHz}$ at $z \simeq 10$) absorptions. At such circumstances broad-band observations are to be more suitable for inferring physical conditions of the absorbing gas. X-ray photons from stellar activity of initial episodes of star formation can compete the contribution from decaying DM only at $z < 10$. Therefore, when observed the 21 cm signal will allow to follow evolution of decaying DM particles in the redshift range $z = 10 - 15$. Contrary, in case of non-detection of the 21 cm signal in the frequency range $\nu < 140 \text{ MHz}$ a lower limit on the ionization rate from decaying dark matter can be established.

Subject headings: early Universe – cosmology: theory – dark matter – diffuse radiation – line: formation - radio lines: general

1. INTRODUCTION

The standard 21-cm tomography of the Universe through observations of emission or absorption from the neutral intergalactic medium (IGM) against the cosmic microwave background (CMB) (Shaver *et al.* 1999; Sethi 2005), and statistical studies of angular distribution of the 21 cm intensity (Tozzi *et al.* 2000; Iliev *et al.* 2002), are known to suffer limitations from yet insufficient angular resolution of the existing and future radiotelescopes: e.g., only few arcseconds in the frequency range of interest ($\sim 150 \text{ MHz}$) on LOFAR¹, which allows to distinguish only about hundreds of comoving kpc. Therefore only huge structures, such as for example, HII regions formed by stellar clusters and quasars, and the large scale domain structure seem possible to be resolved. On the contrary, measurements of absorptions in the 21 cm line to distant quasars – the “21 cm forest” (Carilli *et al.* 2002; Furlanetto & Loeb 2002) – is thought to provide information on small scale structures, such as individual dark matter minihalos, low mass galaxies and even stellar HII regions in the early Universe (Kumar *et al.* 1995; Bagla *et al.* 1997; Furlanetto & Loeb 2002; Furlanetto 2006; Yue *et al.* 2009; Mack & Wyithe 2011). If so the 21 cm forest would serve as a promising tool for studying the very beginning of the reionization epoch, when HII regions from different star forming minihalos have not yet had overlapped.

Detailed study of the line profiles in the 21 cm forest has therefore attracted recently much attention. In particular, dynamical effects on to the line profile from baryon accretion (Xu *et al.* 2011), and from overall contraction during the formation of the minihalos (Meiksin

2011; Vasiliev & Shchekinov 2012) have been recently accounted, contrary to a fully static model with fixed dark matter and baryonic profiles described initially in (Furlanetto & Loeb 2002; Furlanetto 2006). Moreover, the 21 cm forest signal seems to carry information on spatial distribution of dark matter in minihalos, and thus can shed light on ongoing discussion on whether dark matter profiles in minihalos are cuspy as shown first in (Navarro *et al.* 1997), or not as inferred by (Burkert 1995) from observations of local dwarf galaxies. The discussion has been recently exacerbated, on one side, by finding a steepening of the inner-slope of dark matter profiles in the higher mass ellipticals in clusters (Sommer-Larsen & Limousin 2010; Gnedin 2011), and on the other, a flattening of profiles in the first protogalaxies, (Mashchenko *et al.* 2006; Tonini *et al.* 2006; Mikheeva *et al.* 2007). Detailed consideration of characteristics of the 21 cm forest to firmly probe dark matter profiles at early epochs is therefore needed.

Considerable contamination can however come from stellar UV photons (Yue *et al.* 2009; Xu *et al.* 2011) that ionize and heat gas in minihalos. Similar effects are expected from ionizing photons produced by decaying DM particles (Sciama 1982; Scott *et al.* 1991; Bharadwaj & Sethi 1998; Chen & Kamionkowski 2004; Hansen & Haiman 2004; Kasuya & Kawasaki 2004; Kasuya *et al.* 2004; Pierpaoli 2004; Belikov & Hooper 2009), annihilation of dark matter (Chuzhoy 2008; Myers & Nusser 2008; Yuan *et al.* 2010; Cumberbatch *et al.* 2010) and ultra-high energy cosmic rays originating from decaying superheavy ($M_X \gtrsim 10^{12} \text{ GeV}$) DM particles (Berezinsky *et al.* 1997; Birkel & Sarkar 1998; Kuzmin & Rubakov 1998; Doroshkevich & Naselsky 2002; Doroshkevich *et al.* 2003). The background radiation from these sources

Electronic address: eugstar@mail.ru, yus@sfedu.ru

¹ <http://www.lofar.org/index.htm>

can change thermal and ionization evolution of the intergalactic medium (Dodelson & Jubas 1994; Biermann & Kusenko 2006; Shchekinov & Vasiliev 2004; Vasiliev & Shchekinov 2006; Mapelli *et al.* 2006), and affect through it the 21 cm global signal and fluctuations (Furlanetto *et al.* 2006; Shchekinov & Vasiliev 2007; Chuzhoy 2008; Myers & Nusser 2008; Yuan *et al.* 2010; Cumberbatch *et al.* 2010; Natarajan & Schwarz 2009). More recently these sources have been strongly constrained (Zhang *et al.* 2007; Cirelli *et al.* 2009; DeLope Amigo *et al.* 2009; Peter *et al.* 2010; Zhang *et al.* 2010; Galli *et al.* 2011; Hütsi *et al.* 2011), though not fully excluded. In this paper we focus therefore on whether the imprints from them can be recognized in the 21 cm forest absorptions.

We assume a Λ CDM cosmology with the parameters $(\Omega_0, \Omega_\Lambda, \Omega_m, \Omega_b, h) = (1.0, 0.76, 0.24, 0.041, 0.73)$ (Spergel *et al.* 2007), for minihalos we assume a flat dark matter profile.

2. MODEL DESCRIPTION

2.1. Evolution

Dark matter profiles are described as suggested by Ripamonti (2007): the dark matter of $M_{DM} = \Omega_{DM} M_{halo} / \Omega_M$ is a truncated isothermal sphere with the truncation radius R_{tr} evolving as in Tegmark *et al.* (1997), and a flat core of radius R_{core} ; the ratio $\eta = R_{core} / R_{vir}$ is assumed 0.1 through simulations, as commonly used to mimic the evolution of a simple top-hat fluctuation (e.g. Padmanabhan 1993). Dynamics of baryons is described by a 1D Lagrangian scheme similar to that proposed by Thoul & Weinberg (1995); a reasonable convergence is found at a resolution of 1000 zones over the computational domain.

Chemical and ionization composition includes a standard set of species: H, H⁺, H⁻, He, He⁺, He⁺⁺, H₂, H₂⁺, D, D⁺, D⁻, HD, HD⁺ and *e*, with the corresponding reaction rates from (Galli & Palla 1998; Stancil *et al.* 1998). Energy equation includes radiative losses typical in primordial plasma: Compton cooling, recombination and bremsstrahlung radiation, collisional excitation of HI (Cen 1992), H₂ (Galli & Palla 1998) and HD (Flower 2000; Lipovka *et al.* 2005).

Calculations start at redshift $z = 100$. The initial parameters: gas temperature, chemical composition and other quantities – are taken from simple one-zone calculations begun at $z = 1000$ with typical values taken at the end of recombination: $T_{gas} = T_{CMB}$, $x[\text{H}] = 0.9328$, $x[\text{H}^+] = 0.0672$, $x[\text{D}] = 2.3 \times 10^{-5}$, $x[\text{D}^+] = 1.68 \times 10^{-6}$ (see references and details in Ripamonti 2007, Table 2).

2.2. Ionization and heating

Decaying DM contributes into ionization and heating of baryons (see for recent discussion in Bertone 2010). The nature of decaying dark matter particles as well as the decay products are still under debates. Several candidates have been proposed: superheavy particles (Bertone *et al.* 2005), axions (Boehm & Fayet 2004; Boehm *et al.* 2004), sterile neutrinos (Dodelson & Widrow 1994; Hansen & Haiman 2004), weakly interacting massive particles (WIMPs, e.g. Jungman *et al.* 1996). The expected mass regime may

range from very light of few keV (as sterile neutrino) and relatively light of few GeV (e.g. Chen & Kamionkowski 2004), to very heavy – several TeV, as recently discussed by Valdés *et al.* (2012). Depending on the nature of the decaying particle, the decay products may include γ -photons, electrons, positrons and other more exotic particles. For example, detection of positrons of tens of GeV by the PAMELA (Adriani *et al.* 2009) can be explained by the injection from annihilation and/or decay of dark matter (He 2009; Nardi *et al.* 2009). It is clear however that through formation of particle showers the decays end when weakly interacting stable particles escape, while the other couple to baryons via electromagnetic interactions, ionize them and deposit energy.

The most generic form for the ionization rate from decaying DM particle is proposed by (Chen & Kamionkowski 2004)

$$I_e(z) = \chi_i f_x \Gamma_X \frac{m_p c^2}{h\nu_c} \quad (1)$$

where χ_i is the energy fraction deposited into ionization (Shull & van Steenberg 1985), m_p is the proton mass, $f_x = \Omega_X(z) / \Omega_b(z)$, $\Omega_b(z)$, the baryon density parameter, $\Omega_X(z)$, the fractional abundance of decaying particles, Γ_X is the decay rate, $h\nu_c$, the energy of Ly-c photons. It is obvious that the contribution from decaying DM is determined by the product $\xi_i = \chi_i f_x \Gamma_X$ which masks the nature of dark matter particles.

The corresponding heating rate can be written in the form (Chen & Kamionkowski 2004)

$$K = \xi_h m_p c^2 \quad (2)$$

where $\xi_h = \chi_h f_x \Gamma_X$, χ_h is the energy fraction depositing into heating. By order of magnitude $\chi_i \sim \chi_h \sim 1/3$ for the conditions we are interested in (Shull & van Steenberg 1985).

Using the CMB datasets Zhang *et al.* (2007) have constrained the ionization rate associated with radiatively decaying dark matter as $\xi \lesssim 1.7 \times 10^{-25} \text{ s}^{-1}$. An extended analysis of the data of Type Ia supernova, Ly α forest, large scale structure and weak lensing observations have lead DeLope Amigo *et al.* (2009) to a stronger constraint: $\xi \lesssim \xi_L = 0.59 \times 10^{-25} \text{ s}^{-1}$. It is worth noting that all datasets favor long-living decaying dark matter particles with the lifetime $\Gamma_X^{-1} \gtrsim 100 \text{ Gyr}$ (DeLope Amigo *et al.* 2009). Further improvement is expected from the Planck satellite. In this paper we consider models with the ionization rate within this limitation $\xi \leq \xi_L$. As will be seen below such a constraint does not affect understanding of what would happen outside the limit $\xi > \xi_L$.

Equations (1) and (2) are written in assumption of a uniform production of ionizing photons by decaying DM with the density Ω_X without accounting its concentration in minihalos. Virialized minihalos are transparent for sufficiently energetic photons for which $\tau(E) = r_{vir} n_{vir} \sigma(E) < 1$, where r_{vir} and n_{vir} are the radius and the mean density of a virialized halo, $\sigma(E)$ is the photoionization cross-section. The corresponding lower energy of escaping photons is thus

$$E_l \gtrsim 300 \text{ eV} \left(\frac{M}{10^8 M_\odot} \right)^{1/9} \left(\frac{1+z}{10} \right)^{2/3}. \quad (3)$$

In this sense our estimates correspond to a lower limit of ionization and heating rates.

The upper energy limit for the photons able to heat and ionize the IGM is determined such that they are absorbed in the IGM within the Hubble time, and can be readily estimated as $E_u \lesssim 30$ keV (for a detailed description of the “transparency window” see in Chen & Kamionkowski 2004). In the energy range $E_l < E < E_u$ photons are supposed to fill the IGM homogeneously except relatively small circumgalactic regions. Note in this connection that even though each minihalo is a source of ionizing photons, their influence on the circumhalo baryons is obviously negligible because of a very low optical depth $\tau(E)$ at the energies of interest.

Contrary to decaying DM stellar and quasi-stellar sources of ionizing radiation emerge only at redshifts $z < 20$. In addition, they heat nearby surrounding gas, which then emits in 21 cm with a patchy, spot-like distribution on the sky, and thus the imprints from nonstellar and stellar sources can be discriminated (see discussion below in Sect. 4).

2.3. 21 cm: optical depth and equivalent width

The spin temperature of the HI 21 cm line is determined by atomic collisions and scattering of ultraviolet (UV) photons (Field 1958; Wouthuysen 1952). In our calculations we used collisional coefficients from Kuhlen *et al.* (2006) and Liszt (2001). In general, decaying DM deposit into the budget of Ly α photons due to recombinations. However, in our present calculations we neglect UV Ly α -pumping because it is small compare to collisional processes for suitable parameters of the decaying DM and the redshifts of interest (see discussion in Shchekinov & Vasiliev 2007). Moreover, the contribution from stellar Ly α background is small due to a sparsity of first stellar objects at redshifts $z = 10 - 15$.

The optical depth along a line of sight at the frequency ν is

$$\tau_\nu = \frac{3h_p c^3 A_{10}}{32\pi k \nu_0^2} \int_{-\infty}^{\infty} dx \frac{n_{HI}(r)}{\sqrt{\pi} b^2(r) T_s(r)} \exp \left[-\frac{[v(\nu) - v_l(r)]^2}{b^2(r)} \right] \quad (4)$$

where $r^2 = (\alpha r_{vir})^2 + x^2$, $\alpha = r_\perp / r_{vir}$ is the dimensionless impact parameter, $v(\nu) = c(\nu - \nu_0) / \nu_0$, $v_l(r)$ is the infall velocity projected on the line of sight, $b^2 = 2kT_k(r) / m_p$ is the Doppler parameter.

The observed line equivalent width is determined as $W_\nu^{obs} = W_\nu / (1 + z)$, where the intrinsic equivalent width is

$$\frac{W_\nu}{2} = \int_{\nu_0}^{\infty} (1 - e^{-\tau_\nu}) d\nu - \int_{\nu_0}^{\infty} (1 - e^{-\tau_{IGM}}) d\nu \quad (5)$$

where τ_{IGM} is the optical depth of the background neutral IGM.

3. RESULTS

3.1. Dynamics of minihalos

We consider here only evolving minihalos with masses in the range $M = 10^5 - 10^7 M_\odot$ virialized at $z_v = 10$. At

lower redshifts reionization by stellar and quasi-stellar sources comes in to play and contaminate the effects from decaying DM, while on the other hand, at higher redshifts the number of bright background radio sources decreases. The choice of the halo mass range is motivated by the fact that halos of $M = 10^5 M_\odot$ lie below the limit where the baryons can efficiently cool and form stars. Only inside minihalos with $M \gtrsim 2 \times 10^6 M_\odot$ star formation can potentially occur in the sense that they collapse at $z_{vir} = 10$, i.e. the gas density in the most inner shell reaches the critical value 10^8 cm^{-3} when 3-body reactions turn on to form H₂ (Ripamonti 2007). On the other side, minihalos of $M = 10^7 M_\odot$ do eventually collapse and form stars and thus represent the opposite dynamical regime. The results we present here illustrate therefore the typical features of 21 cm absorptions produced by non-starforming ($M = 10^5 M_\odot$), marginally starforming ($M = 10^6 M_\odot$) and starforming ($M = 10^7 M_\odot$) minihalos.

Heating from decaying dark matter (hereafter, DDM heating) weakens the accretion rate of baryons on to minihalos. Therefore, in comparison with the evolution of minihalos in the standard scenario one can expect smaller baryon mass and higher temperature within the virial radius of a minihalo. The influence of decaying particles depends on the minihalo mass and the rate of the decay energy deposited in gas, ξ .

Figure 1 show radial profiles of density (upper), temperature (upper middle), velocity (lower middle) and ionized hydrogen fraction (lower panels) in minihalos $M = 10^5, 10^6, 10^7 M_\odot$ virialized at $z_{vir} = 10$, (from left to right panels, correspondingly); 21 cm absorption profiles from collapsing minihalos the standard recombination model can be found in (Vasiliev & Shchekinov 2012). It is clearly seen that the IGM temperature under DDM heating can approach or even exceed the virial temperature of minihalos: DDM with $\xi \gtrsim 0.1 \xi_L$ heats the IGM up to $T \simeq 250$ K which is only half of the virial temperature of a $M = 10^5 M_\odot$ halo, while $\xi \gtrsim 0.3 \xi_L$ elevates the IGM temperature close to the virial temperature of $M = 10^6 M_\odot$ minihalos. It results in weakening of baryon accretion. Thus the most obvious and important difference between evolving minihalos in the standard recombination regime and the presence of decaying dark matter is the absence of an accretion shock wave in minihalos with $M \lesssim 10^6 M_\odot$, as obviously seen on the lower panels of Figure 1.

The radial density, temperature and velocity profiles in small mass ($M \lesssim 10^6 M_\odot$) minihalos in the presence of DDM heating look similar. The profiles² in massive halos ($M = 10^7 M_\odot$) remain close to those in the standard recombination scenario (see dash lines in Figure 1) inspite of a strong DDM heating. Thus contrary to the halos of smaller mass where gravitation is too weak to overcome additional heating, massive halos, $M \geq 10^7 M_\odot$, instead remain able to support the accretion rate on a practically unchanged level. It is obvious that within the limit $\xi \leq \xi_L$ minihalos with $M = 10^7 M_\odot$ represent the least massive halos sensitive to an additional from DDM. However, as readily seen, further increase of ξ re-

² As for minihalos with $M = 10^7 M_\odot$ the collapse occurs earlier than formal virialization, we present the results for not later than the collapse redshift, i.e. for $z = 11$.

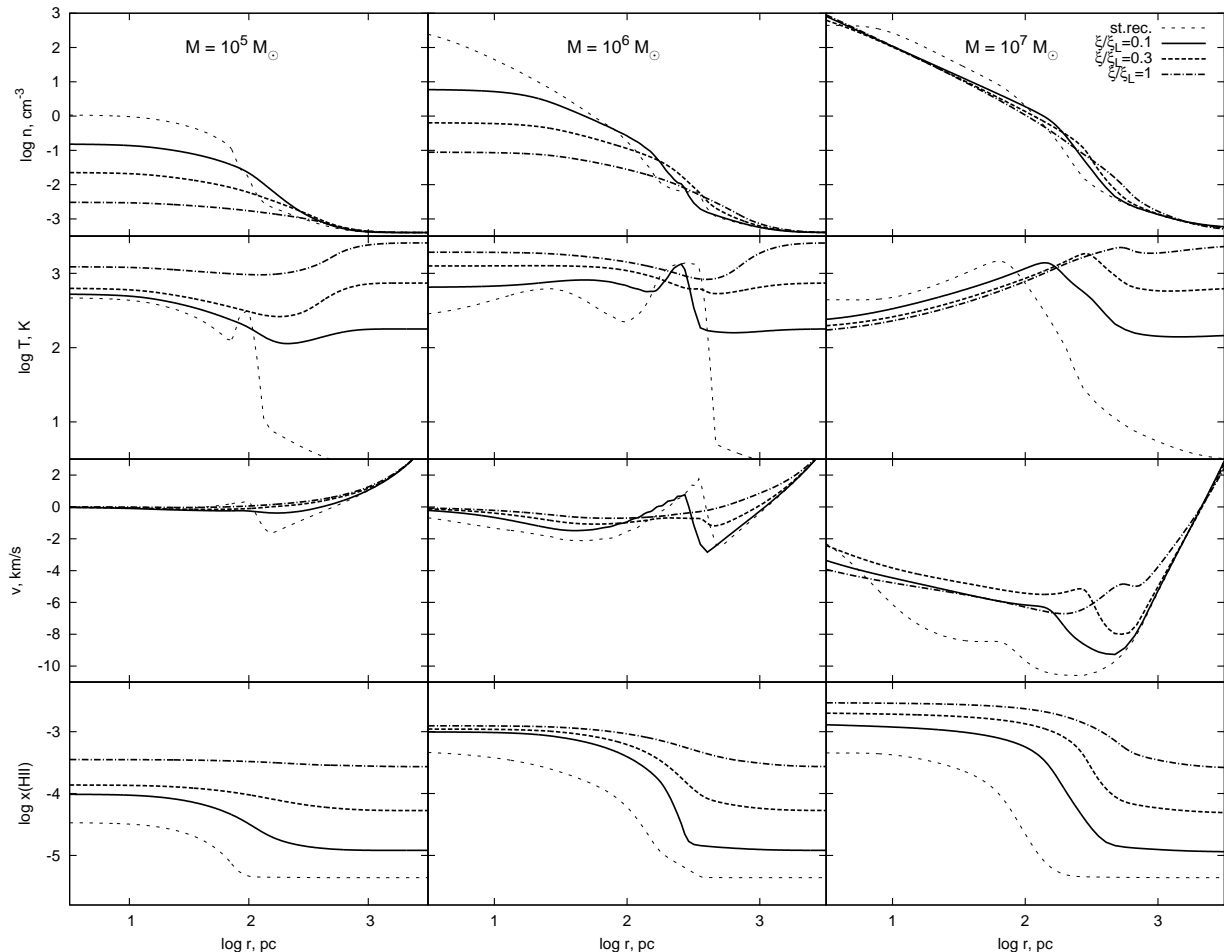


FIG. 1.— The radial density (upper), temperature (upper middle), velocity (lower middle) and ionized hydrogen fraction (lower panels) profiles of halos $M = 10^5 M_\odot$, $10^6 M_\odot$, $10^7 M_\odot$ (from left to right panels, correspondingly) virialized at $z_{vir} = 10$ in the standard recombination model (dots) and in the presence of decaying dark matter with $\xi/\xi_L = 0.1, 0.3, 1$ (solid, dash and dot-dashed lines, correspondingly).

sults in a practically proportional growth of the IGM temperature $T_{IGM} \propto \xi$, and consequently suppresses the accretion rate approximately as $T_{IGM}^{-3/2}$, which in turn increases the lower limit of halo mass insensitive to DDM heating.

Ionization from the decaying DM is considerable: it is seen from Fig. 1 that in the low-mass range ($M \leq 10^6 M_\odot$) the fractional ionization within minihalos and outside them is nearly invariant in models with $\xi \gtrsim 0.3\xi_L$. The ionization rate of $\sim 10\xi_L$ can affect the evolution of minihalos with masses of classical dwarf galaxies $M \sim 10^9 M_\odot$.

3.2. Optical depth

New evolutionary features of minihalos introduced by decaying dark matter are to be manifested in optical depths and equivalent widths of the 21 cm line. Figure 2 shows the maps of optical depth on the “impact parameter – frequency” plane in the standard recombination model (left column of panels) and in the presence of decaying DM with $\xi/\xi_L = 0.1$. The analysis of optical depth in the 21 cm line from minihalos in the standard recombination scenario can be found in (Xu *et al.* 2011; Meiksin 2011; Vasiliev & Shchekinov 2012), so here we will speak only about the models with decaying DM. In

addition, we will discuss only models with a single value of ξ because the other are either similar or have no remarkable features and can be readily scaled.

An obvious result is that decaying DM heavily suppresses optical depth. In the low-mass end $M = 10^5 - 10^6 M_\odot$ the center of line optical depth ($\nu - \nu_0 \lesssim 10$ kHz) for small impact factors ($\alpha \lesssim 0.5$) at $\xi = 0.1\xi_L$ is less than half as compared to the standard case. A small peak in optical depth at $\nu - \nu_0 \simeq 40$ kHz for $M = 10^5 M_\odot$ disappears (the origin of this peak is discussed in Vasiliev & Shchekinov 2012). At a higher impact factor $\alpha \gtrsim 1$ the optical depth remains insensitive to $\xi \lesssim 0.1\xi_L$. However, higher ξ can suppress optical depth down to the background value $\tau \sim 10^{-3}$ for all α : for $M = 10^5 M_\odot$ this occurs when $\xi \gtrsim 0.3\xi_L$, and for $M = 10^6 M_\odot$ it can be met for $\xi \gtrsim \xi_L$. Thus, the decaying DM with $\xi \gtrsim 0.3\xi_L$ practically erases 21 cm absorption features from small mass minihalos.

Massive minihalos, $M = 10^7 M_\odot$, demonstrate more complex frequency-dependence of the optical depth: it does not peak in the center of line, the maximum is instead at $\nu - \nu_0 \sim 45 - 50$ kHz. Such a horn-like dependence originates from a strong accretion in massive halos (Xu *et al.* 2011; Vasiliev & Shchekinov 2012). In the presence of decaying dark matter the range of

TABLE 1
OPTICAL DEPTH IN THE CENTER OF LINE AT VIRIALIZATION

M, M_\odot	$\xi/\xi_L = 0$	$\xi/\xi_L = 0.1$	$\xi/\xi_L = 0.1, I_e = 0$	$\xi/\xi_L = 0.1, K = 0$
10^5	0.15	0.074	0.09	0.12
10^6	0.37	0.074	0.083	0.33
10^7	0.068	0.1	0.081	0.078

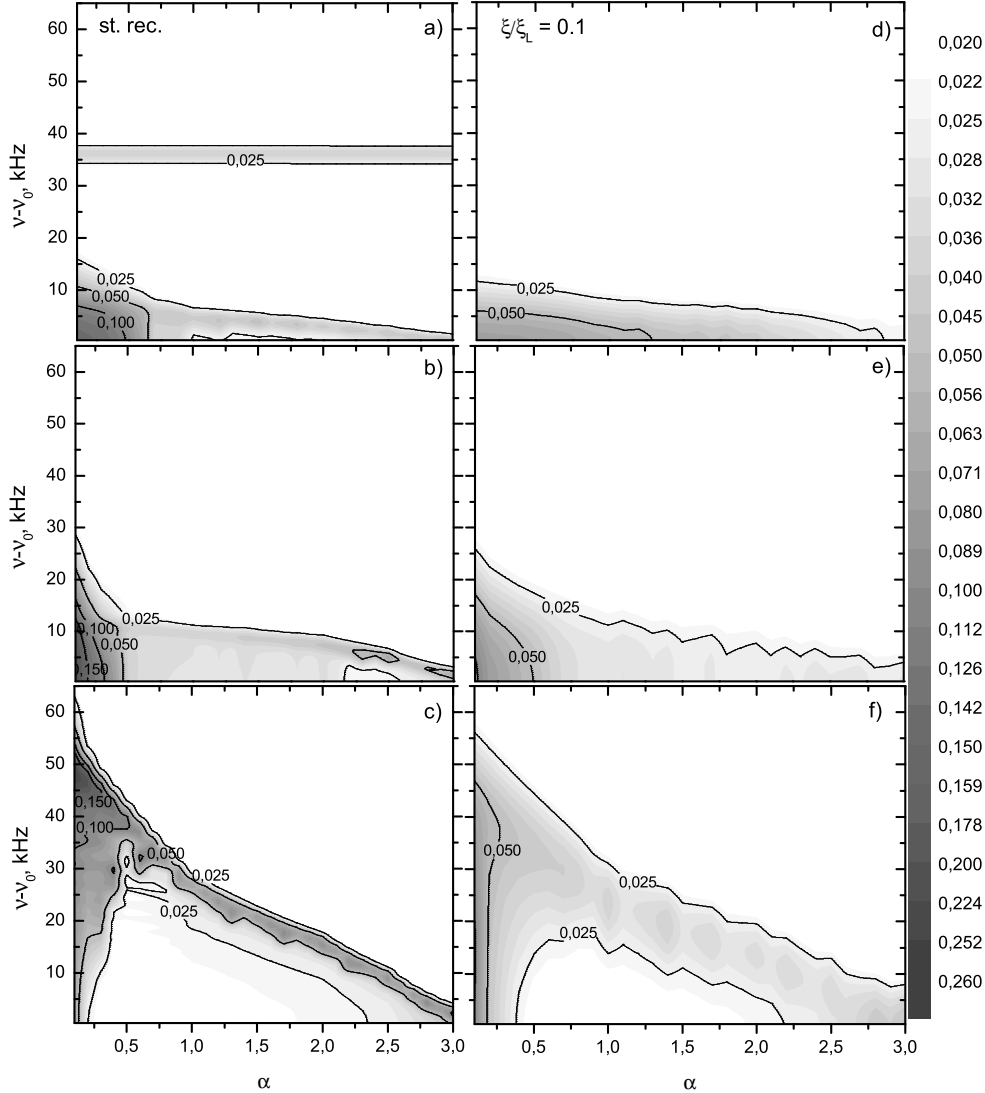


FIG. 2.— The dependence of the 21cm optical depth on frequency and impact parameter $\alpha = r_\perp/r_{vir}$ for halos $M = 10^5 M_\odot$, $10^6 M_\odot$, $10^7 M_\odot$ (from top to bottom, correspondingly) virialized at $z_{vir} = 10$, in the standard recombination model (left column of panels) and in the presence of decaying dark matter with $\xi/\xi_L = 0.1$ (right column).

impact factors with a horn-like profile heavily shrinks even for $\xi \sim 0.1\xi_L$. The centre of line optical depth ($\nu - \nu_0 \lesssim 30$ kHz) at small $\alpha \lesssim 0.1$ becomes flat and insensitive to ξ : it stays at the level ~ 0.05 even for $\sim \xi_L$. At higher α the optical depth merges to the background value.

It is clear that both the heating and the ionization from the decaying DM contribute to the decrease of optical depth. In order to evaluate their relative contributions we performed calculations of two sets of models: in the first set we turned off the ionization from the decay-

ing DM $I_e = 0$ leaving the heating unchanged, while in the second set the ionization remains unchanged, while heating is turned off $K = 0$. The results are shown in Table 1, where the first column shows the center-of-line optical depths τ_0 in the standard ionization scenario, in the second column τ_0 is shown for the model with the decaying DM particles treated self-consistently, the second and the third columns correspond to the models with $I_e = 0$ and K unchanged, and I_e unchanged and $K = 0$, respectively. An obvious trend of increased τ_0 in the shortened models with either $I_e = 0$ or $K = 0$

is caused by an inhibition of the total contribution from the decaying DM. It is also clearly seen that the influence of the ionization I_e is mainly not due to a decrease of the fraction of HI in virialized halos which is negligibly small: $\Delta x(\text{HI}) = -x(\text{HII}) \sim -10^{-3}$. It stems predominantly from an enhanced Compton heating beginning from the turnaround point. Therefore both the ionization and the heating decrease the optical depth via the additional heating. Separate contributions from them depend on the minihalo mass: for instance, for $10^5 M_\odot$ halos they comprise approximately 1/3 for the ionization and 2/3 for the heating, although their contributions are not independent and the combined influence is not simply a sum of the two separate: the additional heating from these sources change the temperature, density and velocity profiles which are involved in the optical depth (4) nonlinearly.

3.3. Equivalent width

Figure 3 demonstrates evolution of the radial profiles of the equivalent widths measured at the observer's rest-frame. As expected it decreases significantly with ξ except those for the halos of $M = 10^7 M_\odot$: for instance, low-mass halos $M = 10^5 M_\odot$ at $z = 10$ (solid lines) show decrease of W_ν^{obs} from ~ 0.2 kHz for the standard recombination to a negligible value $\lesssim 0.02$ kHz for $\xi \geq 0.3\xi_L$ within $r_\perp/r_{\text{vir}} \lesssim 0.5$. At $z = 15.5, 12$ (dash and dot-dash lines) W_ν^{obs} hardly can be resolved on future telescopes and may only deposit into the total signal in broad-band observations (Xu *et al.* 2011).

More massive halos – $M \gtrsim 10^6 M_\odot$, show near the virialization ($z = 10$) strong equivalent widths $W_\nu^{\text{obs}} \gtrsim 0.2$ kHz even at a relatively high ionization $\xi \lesssim 0.3\xi_L$ within the whole halo $\alpha \lesssim 1$, at $\alpha \lesssim 0.5$ W_ν^{obs} can reach even $\sim 0.5 - 0.9$ kHz. In the higher redshift range, $z = 15.5, 12$, $M \gtrsim 10^6 M_\odot$ can produce such strong only in the standard recombination scenario. More massive halos, $M = 10^7 M_\odot$, form strong absorptions ($W_\nu^{\text{obs}} \gtrsim 0.5$ kHz) even for high ionization rate $\xi \sim \xi_L$, though only in a narrow range of impact factor $\alpha \lesssim 0.1$. As a consequence, the decaying DM leads to a considerable decrease of the number of strong absorption lines: for $\xi \gtrsim 0.3\xi_L$ sufficiently strong lines form only in high-mass ($M \geq 10^7 M_\odot$) halos nearly along the diameter with a small probability to contribute into absorptions. Similar effect stems from the action of the stellar X-ray background at lower redshifts (Furlanetto & Loeb 2002; Xu *et al.* 2011), see also Sec. 4.

The sensitivity of future telescopes is at least an order of magnitude lower than the flux limit needed to separate spectral lines from individual halos, i.e. to observe with spectral resolution of $\Delta\nu \sim 1$ kHz. Therefore, Xu *et al.* (2011) have proposed broadband observations with lower resolution. In this case the measured quantity is the average signal from different halos lying on a line of sight. Accordingly, we introduce a radially averaged equivalent width

$$\langle W_\nu^{\text{obs}} \rangle = \frac{2}{9} \int_0^{3r_{\text{vir}}} \frac{W_\nu^{\text{obs}}(r_\perp) r_\perp dr_\perp}{r_{\text{vir}}^2}. \quad (6)$$

Figure 4 presents the dependence of $\langle W_\nu^{\text{obs}} \rangle$ on ξ/ξ_L . The increase of $\langle W_\nu^{\text{obs}} \rangle$ for $M = 10^5 M_\odot$ at $z = 10$ and

$\xi/\xi_L \leq 0.1$ is explained by a widening of W_ν^{obs} in the peripheric region $r_\perp/r_{\text{vir}} \lesssim 2$ (upper panels in Figure 3). For higher masses and redshifts the radially averaged W_ν^{obs} decreases with ξ/ξ_L by factor of $\lesssim 2$ and apparently remains sufficient to distinguish effects from the ionization caused by decaying DM particles.

In previous studies theoretical spectrum of the 21 cm forest has been simulated within the assumption of steady-state minihalos with fixed profiles corresponding to the virialization (Furlanetto & Loeb 2002; Xu *et al.* 2011). When dynamics is taken into account, minihalos lying on a given line of sight are, in general, at different evolutionary stages, and have different density, velocity and temperature profiles. Moreover, Press-Schechter formalism cannot anymore be used for description of their mass function as soon as they are lying far from the virialization. It makes problematic to describe correctly the number density of minihalos at each evolutionary stage. An additional complication stems from continuous structure formation. While major mergers involving merging minihalos with $M \gtrsim 0.5M_h$ occur on times as long as twice of the Hubble time at $z = 10$, less destructive mergers with $M \lesssim 0.25M_h$ proceed within $\lesssim 0.7$ of the Hubble time (Lacey & Cole 1993). This time is shorter than free-fall time in halos with $M \sim 2 \times 10^6 M_\odot$, thus making estimates based on the assumption of the virial equilibrium unapplicable to less massive halos. Possible formation of stars in massive evolved minihalos also introduces additional complication. Overall, the analysis of theoretical spectrum within a statistical simulation becomes exceedingly cumbersome. More relevant picture can be obtained from high-resolution cosmological gas dynamic simulation, although current resolution with $\Delta M \sim 10^6 M_\odot$ seems not to be sufficient.

However, with the upcoming low frequency interferometers (LOFAR and SKA) such modeling is apparently excessive. Indeed, the absorption line profiles and the spectral features from separate minihalos located at $z = 10$ are of 1 to 5 kHz in width – close to the spectral resolution limit 1 kHz. As mentioned in (Xu *et al.* 2011) the corresponding sensitivity requires enormously bright background sources. In order to resolve spectral lines of $\Delta\nu \sim 1$ kHz with a typical for the SKA telescope ratio of the aperture-to-system temperature $A_{\text{eff}}/T_{\text{sys}} = 5000 \text{ m}^2 \text{ K}^{-1}$ and a signal-to-noise ratio $S/N = 5$ the integration time ~ 30 days and the minimum flux density about $500 \mu\text{Jy}$ are needed (Xu *et al.* 2011). This is 4 times lower than the flux density for an object similar to bright radio-loud galaxy Cygnus A (Carilli *et al.* 2002), but an order of magnitude higher than typical GRB afterglow flux (Xu *et al.* 2011). Note, in addition, that there are no confirmed QSOs at $z > 7.5$, and moreover the mass of a black hole in the Cygnus A galaxy is about $2.5 \times 10^9 M_\odot$ (Tadhunter *et al.* 2003), which should apparently be a very rare object at $z \gtrsim 10$. GRB afterglows seem to be more promising background sources for the 21 cm absorption study. In this case the integration time is restricted by the duration of a bright phase of afterglow, ~ 100 days (Frail 2003). Thus, low resolution or broadband observations can be a better alternative.

In broadband observations suppression of optical depth in 21 cm caused by decaying particles manifests as a

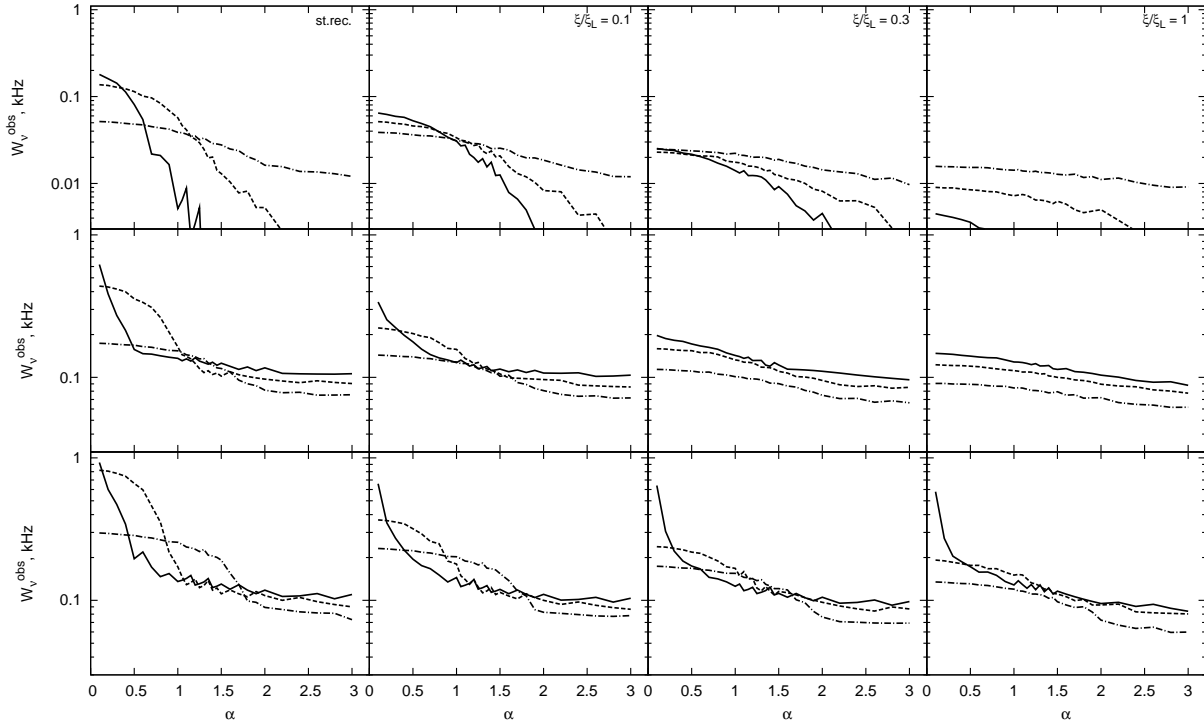


FIG. 3.— The equivalent widths versus the impact parameter α in the observer’s restframe for minihalos with masses $M = 10^5, 10^6, 10^7 M_\odot$ (from top to bottom) at redshifts $z = 15.5, 12$ and $z = z_{vir} = 10$ (dot-dash, dash and solid lines, correspondingly) in the standard recombination model and in the presence of decaying dark matter with $\xi/\xi_L = 0.1, 0.3, 1$ (from left to right, correspondingly). Note that the y -axes are different between the panels.

factor of 2–4 decrease of absorption in the frequency range $\nu < 140$ MHz where contribution from low mass minihalos at $z \geq 10$ dominates. Indeed, the number of halos in the low-mass range $10^5 - 10^7 M_\odot$ at $z = 10$ scales as $n(M, z) \sim M^{-1}$. The probability of minihalos to intersect a line of sight is proportional to $n(M, z) \times (\alpha r_{vir}(M))^2$, resulting in a decrease of the number of strong absorption lines with $W_\nu^{obs} \gtrsim 0.3$ kHz by factor of at least 2.5 for $\xi/\xi_L = 0.3$ and more than 4.5 for $\xi/\xi_L = 1$. Such a decrease inevitably cancels the average 21 cm forest signal from low mass halos. It results in turn in a several times decrease of the mean flux decrement D_A , and correspondingly the detectability limit in broadband observations. Strong suppression of the optical depth at $\xi/\xi_L \gtrsim 0.3$ would require time integration scales longer than the duration of a bright phase of GRB afterglows. Low-mass ($M \sim 10^5 M_\odot$) minihalos produce weak absorptions, $W_\nu^{obs} \lesssim 0.2$ kHz even for the standard ionization scenario.

Thus, as far as the characteristic scales corresponding to such broadband observations are of the order of hundreds of kpc, an immediate consequence is that the advantages expected initially from the 21 cm forest observations become not that obvious. However, once observations are made to cover a wide range of frequencies corresponding to redshifts 10 to 15, they would in principle provide information about how the influence from decaying dark matter varies with redshift. More explicitly, a non-detection of absorptions from 21 cm in the frequency range $\nu < 140$ MHz can in principle serve to bound the ionization rate from decaying DM *from below*: $\xi/\xi_L \gtrsim 0.3$, unless contribution from stellar sources becomes competitive to ionize low mass halos.

4. RELATIVE CONTRIBUTION FROM PARTICLE DECAYS AND STELLAR X-RAY BACKGROUND

As mentioned above the contribution of X-ray photons from decaying particles into ionization and heating of the IGM can compete the one from X-ray produced by early population of binaries and/or black holes. Let us estimate here comparatively these two contributions. For this purpose we assume the X-ray (> 0.2 keV) luminosity of high- z galaxies to be comparable to that inferred for nearby starburst galaxies (Gilfanov *et al.* 2004)

$$L_X = 3.4 \times 10^{40} f_X \left(\frac{SFR}{1 M_\odot \text{ yr}^{-1}} \right) \text{ erg s}^{-1} \quad (7)$$

where SFR is the star formation rate, and f_X is a correction factor accounting for the unknown properties of X-ray emitting sources in the early universe. Rather a weak constraint on f_X inferred from the WMAP CMB optical depth $\lesssim 10^3$ (Pritchard & Loeb 2008) is much higher than found in the nearby universe, $f_X \simeq 0.3 - 1$ (Gilfanov *et al.* 2004; Mineo *et al.* 2012). From the signal in stacked Chandra images at the position of $z \sim 6$ galaxies (Treister *et al.* 2011), the soft X-ray background is argued to limit the f_X factor by $\gtrsim 2 - 5$ at $z \geq 1 - 2$, though allows f_X to increase sharply up to ~ 100 at $z > 5$ (Dijkstra *et al.* 2012). However, further rigorous analysis did not confirm such a high f_X (Willott 2011; Fiore *et al.* 2012), and show that it remains invariant at least within $z = 0 - 4$ (Cowie *et al.* 2012). Thus, no reason are seen to assume f_X much higher than that in the local universe.

Assuming that the star formation rate is proportional to the rate at which matter collapses into galaxies (Furlanetto 2006), the total normalized X-ray emissivity

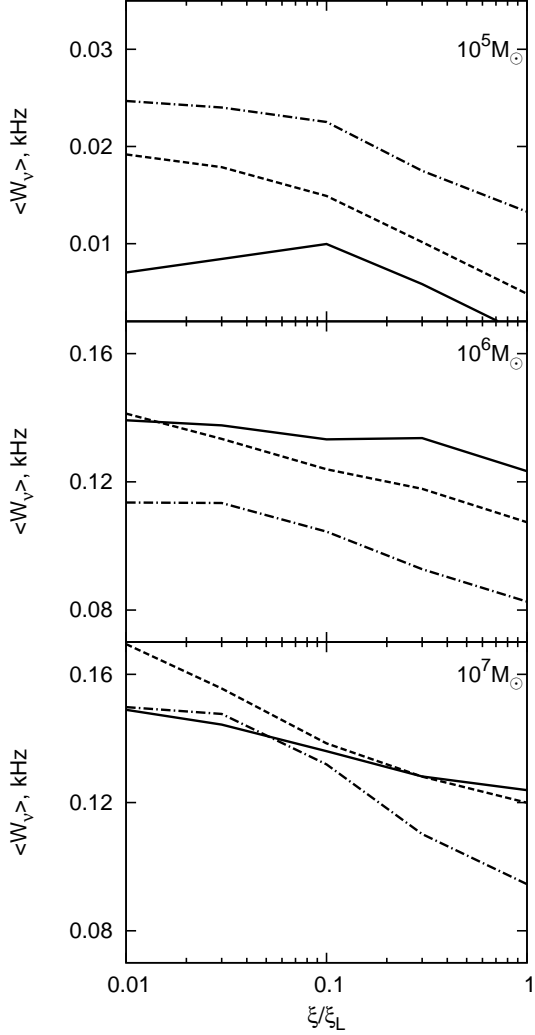


FIG. 4.— The dependence of the radially averaged equivalent width for minihalos with mass $M = 10^5, 10^6 M_{\odot}, 10^7 M_{\odot}$ (from top to bottom panels, correspondingly) at redshifts $z = 15.5, 12$ and 10 (dot-dash, dash and solid lines, correspondingly) on the ionization rate ξ/ξ_L ; in the logarithmic x -axis $\xi/\xi_L = 0.01$ is set to correspond to $\xi/\xi_L = 0$, i.e. the standard recombination. Note differences between the panels on y -axes scales.

ϵ_X can be written as

$$\frac{2\epsilon_X}{3knH(z)} = 5 \times 10^4 f_X \left[\frac{f_*}{0.1} \frac{df_{coll}/dz}{0.01} \frac{1+z}{10} \right], \quad (8)$$

here df_{coll}/dz is the fraction of baryons collapsed to form a protogalaxy per unit redshift, f_* , the fraction of baryons converted into stars in a single star formation event, normalization numbers are given in (Furlanetto 2006). The corresponding heating rate can be found as $K_* = \chi_h \epsilon_X$, which can be now compared to the heating rate associated with decaying particles

$$\frac{2K}{3kH(z)} = 8.9 \times 10^4 (\xi/\xi_L) \left(\frac{1+z}{10} \right)^{-2/3}. \quad (9)$$

The condition that these two sources heat the IGM equally is therefore

$$0.54 f_X \chi_h \left[\frac{f_*}{0.1} \frac{df_{coll}/dz}{0.01} \left(\frac{1+z}{10} \right)^{5/3} \right] = (\xi/\xi_L). \quad (10)$$

Thus, in order that the heating from stellar X-ray background were equal to the heating from decaying particles one would require for the X-ray correction factor $f_X \simeq 5.4(\xi/\xi_L)$ for $1+z = 10$ and typical parameters for the star formation. At $\xi/\xi_L > 0.1$ such value seems to be exceedingly higher than follows from observations of starburst galaxies in the local Universe with $f_X \simeq 0.3$ (Gilfanov *et al.* 2004). Moreover, the linear approximation (7) is valid only for a sufficiently massive systems with the star formation rate $\gtrsim 10 M_{\odot} \text{ yr}^{-1}$, while in the low end of SFR the correction factor can be one to two orders lower. At the redshifts of interests $z \sim 10$ only halos with masses $M_h \lesssim 10^7 M_{\odot}$ can be star-forming (Loeb 2010), for which the SFR is at most $\sim 10^{-3} M_{\odot} \text{ yr}^{-1}$ for typical numbers characterizing the formation of stars in the early Universe: $f_* = 0.1$, $df_{coll}/dz \sim 0.01$. Such a low star formation rate corresponds however to more than factor of 10 weaker proportion between the star formation and the X-ray luminosity, i.e. $f_X \ll 0.1$ (see Fig. 1 in Gilfanov *et al.* 2004). One may conclude therefore that at redshifts $z \geq 10$ heating of atomic hydrogen in virializing minihalos can stem only from the decaying particles, unless the star formation efficiency f_* and the amount of a collapsed baryons df_{coll}/dz grows towards higher z unprecedentedly. Without overwhelming assumptions the conclusion about a dominance of decaying particles in heating looks most plausible.

As mentioned above higher f_X can in principle be met at $z \sim 10$ (Dijkstra *et al.* 2012), in which case the contribution from decaying particles decreases at $z \lesssim 10$, though at higher redshifts they still dominate due to an obvious sharp drop of star formation. The different redshift dependence of the stellar X-ray and the decaying particle heating rates (9), may be used to discriminate between them. In general though, both higher ξ and f_X lead to smaller number of absorption lines. As a consequence the decrement D_A decreases, and the integration time increases such that even GRB afterglows cannot serve to observe the 21 cm forest.

It is obvious that strong stellar X-ray sources, such as, e.g., SN remnants or massive X-ray binaries, ionize and heat the IGM locally, even though the X-ray background from them can be weaker than from decaying particles. Indeed, the mean free path of photons with $E \sim 0.3 \text{ keV}$ at $z \sim 10$ is about $1 \text{ Mpc}/(1+\delta)$, where δ is the density perturbation. The heating rate at a distance D from a source with X-ray luminosity L [erg s $^{-1}$] is

$$\Gamma \sim 6 \times 10^{-28} \left(\frac{L}{10^{40}} \right) \left(\frac{10 \text{ kpc}}{D} \right)^2 \chi_h \times \left(\frac{E/E_H}{20} \right)^{-3} \exp(-\tau) \text{ erg s}^{-1}, \quad (11)$$

and the corresponding ionization rate is

$$I \sim 2 \times 10^{-17} \left(\frac{L}{10^{40}} \right) \left(\frac{10 \text{ kpc}}{D} \right)^2 \times \left(\frac{E/E_H}{20} \right)^{-3} \chi_i \exp(-\tau) \text{ s}^{-1}. \quad (12)$$

It is readily seen that in the presence of heating from decaying particles the zone of influence of a star-forming

dwarf galaxy lies within the radius

$$D \lesssim 10 \left(\frac{SFR}{1 M_{\odot} \text{ yr}^{-1}} \right)^{-1/2} (\xi/\xi_L)^{-1/2} \text{ kpc.} \quad (13)$$

As far as a typical distance between minihalos $d \sim 30(1+z/20)$ kpc, only in the beginning of reionization epoch dwarf galaxies can dominate heating and ionization of hydrogen in neighbor minihalos only when the ionization from the background X-ray photons from decaying particles is relatively weak, $(\xi/\xi_L) < 0.1$.

5. CONCLUSIONS

In this paper we have considered the influence of decaying dark matter particles on the HI 21 cm absorption features from low mass minihalos: $M = 10^5, 10^6 M_{\odot}, 10^7 M_{\odot}$, virialized at $z_{vir} = 10$. We used a 1D self-consistent hydrodynamic approach to study their evolution, and followed the absorption characteristics from the turnaround to the virialization of minihalos. We have found that

- due to additional heating from decaying particles thermal and dynamical evolution of minihalos show pronounced differences from those in the model without particle decays (i.e. with the standard recombination scenario), and can be distinguished in the signal formed at redshifts $z > 10$;
- the additional heating and ionization strongly suppress optical depth in the 21 cm line: they practically “erase” the 21 cm absorptions from minihalos with $M = 10^5 - 10^6 M_{\odot}$ even at a relatively modest ($\xi \gtrsim 0.3\xi_L$) ionization rate; the horn-like dependence of the optical depth found for minihalos with $M \sim 10^6 - 10^7 M_{\odot}$ in the standard recombination scenario (Xu *et al.* 2011) almost disappears even at a lower ionization rate $\xi \gtrsim 0.1\xi_L$. In total, approximately 1/3 of this suppress stems from the ionization, while the rest $\sim 2/3$ is due to the heating. The contribution from the ionization is caused by an enhanced Compton heating on additional electrons, rather than by decreased fraction of HI.

- the suppress of the magnitude of 21 cm absorption by the ionization from decaying DM particles, and the widening of the lines by dynamical effects – baryon accretion and dark matter contraction – necessitate broadband observations, in which case the advantages of the 21 cm forest to probe reionization on small scales become less obvious as compared to the traditional 21 cm global signal and 21 cm angular distribution;
- stellar contribution at such redshifts, $z \geq 10$, is negligibly small, so that a weakening of the 21 cm forest if observed can be only due to decaying dark matter particles.
- the equivalent width of the 21 cm absorption line decreases significantly when ξ increases, and the number of strong absorption lines $W_{\nu}^{obs} \gtrsim 0.3$ kHz at $z = 10$ drops by more than 2.5 to 4.5 times depending on ξ ; such a decrease inevitably erases the averaged 21 cm forest signal from low mass halos ($M \sim 10^5 - 10^6 M_{\odot}$, i.e. the frequency range $\nu < 140$ MHz) in future broad-band observations. Within a conservative assumption that f_X does not grow enormously and remains at higher redshifts $z \gtrsim 10$ comparable to its value in the local Universe, such decrease of the EW can be attributed only to the decaying DM. As far as it occurs at $\xi > 0.3\xi_L$ the deficiency of 21 cm forest absorptions at these frequencies can serve to put *a lower limit on the ionization rate from unstable DM*.

The authors thank M. Gilfanov for valuable and helpful comments, the anonymous referee for critical remarks, and Shiv Sethi for discussions. This work is supported by the Federal Agency of Education (project codes RNP 2.1.1/11879). EV acknowledges support from the “Dynasty” foundation, the RFBR through the grant 12-02-00365 and the Russian federal task program Research and operations on priority directions of development of the science and technology complex of Russia for 2009-2013 (state contract 14.A18.21.1304).

REFERENCES

- Adriani O. *et al.*, 2009, Nature 458, 607
 Bagla J.S., Nath B.B., Padmanabhan T., 1997, MNRAS, 289, 571
 Belikov A. V. & Hooper D., 2009, PhRvD, 80c5007
 Berezhinsky V. S., Kachelrieß M. & Vilenkin A., 1997, Phys. Rev. Lett., 79, 4302
 Bertone G., Hooper D., Silk J., 2005, PhR, 405, 279
 Bertone G., 2010, in: Particle Dark Matter : Observations, Models and Searches, ed. G. Bertone, CUP
 Bharadwaj S. & Sethi S., 1998, ApJS, 114, 37
 Biermann P.L. & Kusenko A. 2006, Phys. Rev. Lett. 96i, 1301
 Birkel M. & Sarkar, S., 1998, Astropart. Phys., 9, 298
 Boehm C. & Fayet P., 2004, Nucl. Phys. B 683, 219
 Boehm C., P. Fayet P., Silk J., 2004, Phys. Rev. D 69, 101302
 Burkert A., 1995, ApJ, 447, L25
 Carilli C.L., Gnedin N.Y., Owen F., 2002, ApJ, 577, 22
 Cen R., 1992, ApJ, 78, 341
 Cen R., 2006, ApJ, 648, 47
 Chen, X. & Kamionkowski, M., 2004, Phys. Rev. D, 70, 043502
 Chen X. & Miralda-Escudé J., 2004, ApJ, 602, 1
 Chuzhoy L. 2008, ApJ, 679, 65
 Cirelli M., Iocco F., Panci P., 2009, JCAP, 10, 009
 Cowie L.L., Barger A.J., Hasinger G., 2012, ApJ, 748, 50
 Cumberbatch D. T., Lattanzi M., Silk J., 2010, PhRvD, 82j3508
 DeLope Amigo S., Man-Yin Cheung W., Huang Zh., Ng S.-P., 2009, JCAP, 06, 005
 Dijkstra M., Gilfanov M., Loeb A., Sunyaev R., 2012, MNRAS, 421, 213
 Dodelson S. & Jubas J.M., 1994, MNRAS, 266, 886
 Dodelson S. & Widrow L.M., 1994, Phys. Rev. Lett. 72, 17
 Doroshkevich A.G. & Naselsky P.D., 2002, Phys. Rev. D, 12, 123517
 Doroshkevich A.G., Naselsky I.P., Naselsky P.D., Novikov I.D., 2003, ApJ, 586, 709
 Field G.B., 1958, Proc. IRE, 46, 240
 Fiore F., Puccetti S., Mathur S., 2012, Adv. Astron., 271502
 Flower D., 2000, MNRAS, 318, 875
 Frail D. A., 2003, astro-ph/0309557
 Furlanetto S. R., 2006, MNRAS, 370, 1867
 Furlanetto S.R., Loeb A., 2002, ApJ, 579, 1
 Furlanetto S. R., Oh S. P., Pierpaoli E., 2006a, Phys. Rev. D, 74, 103502
 Galli D. & Palla F., 1998, A&A, 335, 403
 Galli S., Iocco F., Bertone G., Melchiorri A., 2011, PhRvD, 84b7302
 Gilfanov M., Grimm H.-J., Sunyaev R., 2004, MNRAS, 347, L57

- Gnedin O. Y., Ceverino D., Gnedin N. Y., Klypin A. A., Kravtsov A. V., Levine R., Nagai D., Yepes G., 2011, arXiv:1108.5736
- Hansen S. & Haiman Z., 2004, ApJ, 600, 26
- He X. G., Mod. Phys. Lett. A, 2009, 52, 2139
- Hogan C.J. & Rees M.J., 1979, MNRAS, 188, 791
- Hütsi G., Chluba J., Hektor A., Raidal M., 2011, A&A accepted arXiv:1103.2766
- Jungman G., Kamionkowski M., Griest K., 1996, Phys. Rept. 267, 195
- Iliev I.T., Shapiro P.R., Ferrara A., Martel H., 2002, ApJ, 572, 123
- Kasuya S. & Kawasaki M., 2004, Phys. Rev. D, 70, 103519
- Kasuya S., Kawasaki M. & Sugiyama, N., 2004, Phys. Rev. D, 69b, 3512
- Kuhlen M., Madau P., Montgomeri R., 2006, ApJ, 637, 1
- Kumar A., Padmanabhan T., Subramanian K., 1995, MNRAS, 272, 544
- Kuzmin V. A. & Rubakov V. A., 1998, Phys. Atom. Nucl., 61, 1028
- Lacey C. & Cole S., 1993, MNRAS, 262, 627
- Lipovka A., Núñez-López R., Avila-Reese V., 2005, MNRAS, 361, 850
- Liszt H., 2001, A&A, 371, 698
- Loeb A., 2010, How Did the First Stars and Galaxies Form? Princeton Uni. Press
- Mack K. J. & Wyithe J.S.B. 2011, MNRASsubmitted, arXiv1101.5431
- Madau P., Meiskin A., Rees M.J., 1997, ApJ, 475, 492
- Mapelli M., Ferrara A., Pierpaoli E., 2006, MNRAS369, 1719
- Mashchenko S., Couchman H.M.P., Wadsley J., 2006, Nature, 442, 539
- Meiksin A., 2011, MNRAS, 417, 1480
- Mikheeva E.V., Doroshkevich A.G., Lukash V.N., 2007, Nuovo Cim. B, 122, 1393
- Mineo S., Gilfanov M., Sunyaev R., 2012, MNRAS, 426, 1870
- Myers Z. & Nusser A., 2008, MNRAS, 384, 727
- Nardi E., Sannino F., Strumia A, 2009, JCAP, 01, 43
- Natarajan A. & Schwarz D. J. 2009, PhRvD, 80d3529
- Navarro J.F., Frenk C.S., White S.D.M., 1997, ApJ, 490, 493
- Padmanabhan T., 1993, Structure Formation in the Universe, Cambridge Univ. Press, Cambridge
- Peter, A., Moody, C. E., Benson, A. J., Kamionkowski M. 2010, arXiv1011.4970
- Pierpaoli E., Phys. Rev. Lett., 2004, 92, 031301
- Pritchard J. & Loeb A., 2008, Phys. Rev. D., 78, 103511
- Ripamonti E., 2007, MNRAS, 376, 709
- Schaerer D., 2003, A&A, 397, 527
- Sciama, D. W., 1982, MNRAS, 198, 1
- Scott D., Rees M. J., Sciama D., 1991, A&A, 250, 295
- Sethi S., 2005, MNRAS, 363, 818
- Shaver P. A., Windhorst R. A., Madau P., & de Bruyn A. G., 1999, A&A, 345, 380
- Shchekinov Yu. A. & Vasiliev E. O., 2004, A&A, 419, 19
- Shchekinov Yu. A. & Vasiliev E. O., 2007, MNRAS, 379, 1003
- Shull J.M. & van Steenberg M.E. 1985, ApJ, 298, 268
- Sommer-Larsen J., Limousin M., 2010, MNRAS, 408, 1998
- Spergel D. N., Bean R., Doré O. et al., 2007, ApJS, 170, 377
- Stancil P.C., Lepp S., Dalgarno A., 1998, ApJ, 509, 1
- Tadhunter C., Marconi A., Axon D., Wills K., Robinson T.G., Jackson N., 2003, MNRAS, 342, 861
- Tegmark M., Silk J., Rees M. J., Blanchard A., Abel T., Palla F., 1997, ApJ, 474, 1
- Thoul A. & Weinberg D., 1995, ApJ, 442, 480
- Tonini C., Lapi A., Salucci P., 2006 ApJ, 649, 591
- Tozzi P., Madau P., Meiskin A., Rees M.J., 2000, ApJ, 528, 597
- Treister E., Schawinski K., Volonteri M., Natarayan P., Gawiser E., 2011, Nature, 474, 356
- Valdés M., Evoli C., Messinger A., Ferrara A., Yoshida N., 2012, MNRAS, 413
- Vasiliev E. O. & Shchekinov Yu. A., 2006, Astr. Rept., 50, 778
- Vasiliev E. O. & Shchekinov Yu. A., 2012, Astr. Rept., 89, 99
- Willott C.J., 2011, ApJ, 742, L8
- Wouthuysen S. 1952, AJ, 57, 31
- Xu Y., Ferrara A., Chen X., 2011, MNRAS, 410, 2025
- Yuan Q., Yue B., Bi. X.-J., Chen X., Zhang X., 2010, JCAP, 10, 023
- Yue B., Ciardi B., Scannapieco E., Chen X., 2009, MNRAS, 398, 2122
- Zhang L., Chen X., Kamionkowski M., Si Z.-G., Zheng Zh., 2007, PhRvD, 76f1301
- Zhang L., Weniger Ch., Maccione L., Redondo J., Sigl G., 2010, JCAP, 06, 027